ACS OMEGA

http://pubs.acs.org/journal/acsodf

Article

# Reactions of Photoionization-Induced CO−$H_2O$ Cluster: Direct Ab Initio Molecular Dynamics Study

Hiroto Tachikawa*

Cite This: *ACS Omega* 2021, 6, 16688−16695

Read Online

ACCESS | Metrics & More | Article Recommendations | Supporting Information

**ABSTRACT:** The hydrocarboxyl radical (HOCO) is an important species in combustion and astrochemistry because it is easily converted to $CO_2$ after hydrogen reduction. In this study, the formation mechanism of the HOCO radical in a CO−$H_2O$ system was investigated by direct ab initio molecular dynamics calculations. Two reactions were examined for HOCO formation. First, the reaction dynamics of the CO−$H_2O$ cluster cation, following the ionization of the neutral parent cluster $CO(H_2O)_n$ ($n$ = 1−4), were investigated. Second, the bimolecular collision reaction between CO and $(H_2O)_n^+$ was studied. In the ionization of the $CO(H_2O)_n$ clusters ($n$ = 3 and 4), proton transfer, expressed as $CO(H_2O)_n^+ \rightarrow CO-(OH)H_3O^+(H_2O)_{n-2}$, occurred within the $(H_2O)_n^+$ cluster cation, and the HOCO radical was yielded as a product upon addition of CO and OH. This reaction proceeds under zero-point energy. Also, this radical was effectively formed from the collision reaction of CO with water cluster cation $(H_2O)_n^+$, expressed as $CO + OH(H_3O^+)(H_2O)_{n-2} \rightarrow HOCO-H_3O^+ + (H_2O)_{n-2}$. If the intermolecular vibrational stretching mode is excited in the $CO(H_2O)_n$ cluster (vibrational stretching between CO and the water cluster), the HOCO radical was detected after ionization when $n$ = 2. The reaction mechanism was discussed based on the theoretical results.

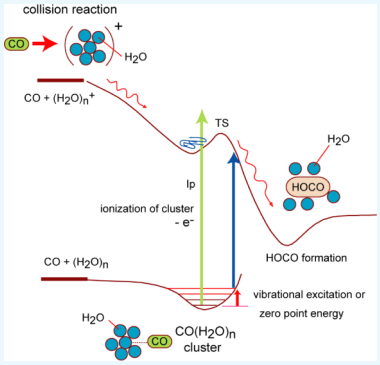


## 1. INTRODUCTION

Superfluid helium droplets have been actively utilized as a new matrix in spectroscopy because molecules can be easily captured and isolated in them.[1−5] Helium droplets provide an unusual nanoscale environment for exploring phenomena at very low temperatures. They typically consist of $10^3$−$10^6$ helium atoms[6] and can be doped with atoms or molecules that are subsequently cooled to the equilibrium temperature of the droplets (0.37 K). Molecules rotate almost freely in helium droplets, and a well-separated spectrum of the rotating state can be obtained. Therefore, it is possible to perform high-resolution spectroscopy of molecules in helium droplets.[7−10]

It is also possible to observe bimolecular reactions if two kinds of molecules are injected into the droplet.[11−13] Fárník and Toennies observed an ion−molecule reaction involving two different molecular constituents in helium droplets.[14] The reactions were initiated by a primary electron impact ionization, and they observed the reactions of $N_2^+$ with $D_2$ and $CH_3^+$ with $D_2$.

In 2011, Liu et al. experimentally investigated the reactions induced by electron impact ionization in helium droplets.[15,16] They synthesized core−shell particles composed of water clusters and dopant molecules in helium droplets. The codopants chosen for investigation were $X$ = CO, Ar, $CO_2$, $O_2$, $N_2$, etc. The products of ionized core−shell particles were analyzed in detail. For $X$ = Ar, $CO_2$, $N_2$, and $O_2$, the parent water cluster cation $(H_2O)_n^+$ was detected after the ionization of $X(H_2O)_n$. In contrast, for $X$ = CO, the protonated water cation $H^+(H_2O)_{n-1}$ was detected after the ionization of $X(H_2O)_n$, indicating that CO behaved in a different manner in helium droplets.

They postulated that the ion−molecule reaction, shown in eq 1 leading to the formation of hydrocarboxyl radical (HOCO), was responsible for the enhanced fragmentation of the water cluster ions in the helium droplet experiments

$$CO + (H_2O)_n^+ \rightarrow H^+(H_2O)_{n-1} + HOCO \quad (1)$$

CO can remove the OH radicals and form stable reaction products as follows:[15]

$$CO + OH \rightarrow HOCO \quad (2)$$

To confirm the reaction mechanism, Shepperson et al.[17] performed ab initio calculations and estimated the energy difference between $HOCO-H^+(H_2O)$ and $CO(H_2O)_2^+$. The former was energetically more stable than the latter, and the reaction energy for the formation of HOCO was significantly large. Hence, they concluded that reaction (eq 1) will be possible in helium droplets.

Lee et al. investigated the reaction mechanism of CO with ionized water dimer cation in detail using ab initio

Received: May 18, 2021
Accepted: June 4, 2021
Published: June 14, 2021

calculations.[18] They calculated the potential energy surface for the formation of HOCO from CO + $(H_2O)_2^+$. They showed that the formation of HOCO from the reaction of CO and $(H_2O)_2^+$ was accompanied by a large exothermic energy. Additionally, they showed the existence of a reaction barrier during the addition of CO and OH in the water dimer cation.

In this study, direct ab initio molecular dynamics (AIMD) calculation[19−21] was performed to study the reaction of $CO(H_2O)_n^+$, following the ionization of parent neutral clusters, to elucidate the mechanism of OH loss in CO−$H_2O$ clusters. Additionally, bimolecular collision reactions between CO and $(H_2O)_n^+$ were investigated for comparison. Figure 1 shows the

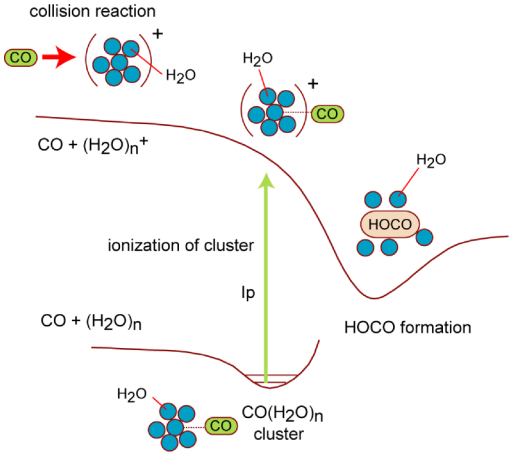


**Figure 1.** Schematic illustration of the potential energy curves of HOCO formation obtained from the calculations in this study: (1) reaction from the $CO(H_2O)_n$ clusters (ionization) and (2) collision reaction of CO and $(H_2O)_n^+$.

concept of the present calculations, in which two reaction channels, namely, the ionization of the $CO(H_2O)_n$ cluster and the bimolecular collision reaction between CO and $(H_2O)_n^+$ were examined. The purpose of this study is to determine the preferred mechanism for the formation of the HOCO radical. Moreover, the reaction time for HOCO formation was determined from the direct AIMD calculations.

The HOCO radical is an important species in astrochemistry. Much of the carbon dioxide ($CO_2$) on Earth and Mars is produced from HOCO. The cosmic ray irradiation of CO−$H_2O$ ice is an important process in the chemistry of various astronomical bodies, ranging from cold interstellar media to comet surfaces. A number of experiments have been carried out in mixtures of CO−$H_2O$ systems.[22−25] The HOCO radical was detected as one of the products in these experiments. Therefore, the study of the formation mechanism of HOCO is strongly correlated to the elucidation of the chemical evolution in the universe.

## 2. COMPUTATIONAL DETAILS

**2.1. Ab Initio Calculations.** The geometries of neutral clusters comprising CO and water molecules, $CO(H_2O)_n$ ($n$ = 1−4), were optimized using the second-order perturbation Møller−Plesset (MP2) method with a 6-311++G(d,p) basis set. The CAM-B3LYP functional was also applied during geometry optimization.[26] For small clusters ($n$ = 2), the coupled-cluster single, double, and perturbative triple excitation (CCSD(T)) method[27] was used for comparison. Atomic and molecular charges were determined from the natural population analysis (NPA). The standard Gaussian 09 program package was used for all static ab initio calculations.[28]

**2.2. Direct AIMD Calculations.** The trajectories of $CO(H_2O)_n^+$, following the ionization of the neutral cluster of $CO(H_2O)_n$, were calculated at the MP2/6-311++G(d,p) level. The excess energy and momentum vector of $CO(H_2O)_n^+$ at the vertical point were assumed to be zero (0 fs). In addition, the effects of the zero-point energy (ZPE) of $CO(H_2O)_n$ ($n$ = 2−4) were examined. The velocity Verlet algorithm, with a time step of 0.01−0.10 fs, was used to solve the equations of motion for the system. The maximum simulation time was 2.0 ps. The total energy drift in all the trajectory calculations was less than 0.01 kcal/mol. Direct AIMD calculations were carried out using our own code.[29−31]

Direct AIMD calculations of the neutral clusters $CO(H_2O)_n$ ($n$ = 1−4) were also carried out under constant temperature conditions (10 K) to generate the initial geometries of the structure in the vertical ionized state, $[CO(H_2O)_n^+]_{ver.}$[32] The Nosé−Hoover algorithm was used to maintain a constant temperature during each trajectory. Direct AIMD calculations of $CO(H_2O)_n^+$ were performed at the CAM-B3LYP/6-311++G(d,p) level. Ten trajectories were run for each cluster size ($n$).

## 3. RESULTS

**3.1. Structures of $CO(H_2O)_n$ Clusters ($n$ = 1−4).** Figure 2 shows the optimized structures of $CO(H_2O)_n$ ($n$ = 1−4)

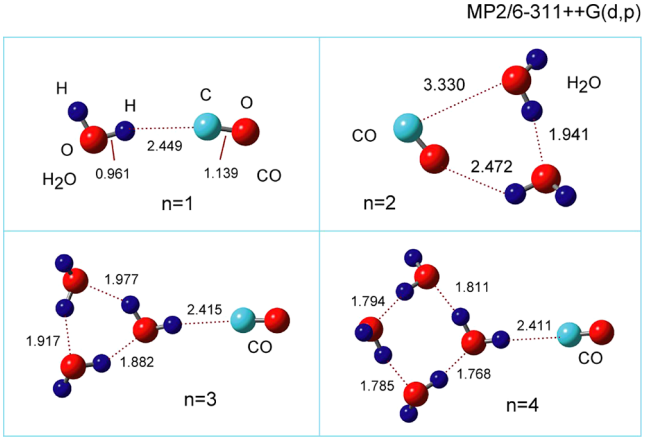


**Figure 2.** Optimized structures of neutral clusters $CO(H_2O)_n$ ($n$ = 1−4) calculated at the MP2/6-311++G(d,p) level. Bond lengths are in Å.

calculated at the MP2/6-311++G(d,p) level of theory. For $n$ = 1, the O−H bond of $H_2O$ is oriented toward the carbon atom of the CO molecule. The intermolecular distance was 2.449 Å, and the binding energy was 1.8 kcal/mol, which is significantly smaller than that of the water dimer (6.1 kcal/mol). For $n$ = 2, the water dimer is oriented toward the CO molecule; the C−O and O−H bond distances were 3.330 and 2.472 Å, respectively. The binding energy for the reaction CO + $(H_2O)_2$ → $CO(H_2O)_2$ was 1.9 kcal/mol. For $n$ = 3, the cyclic water trimer interacted with CO, and the binding energy for the reaction CO + $(H_2O)_3$ → $CO(H_2O)_3$ was 2.0 kcal/mol ($n$ = 3). The cyclic water tetramer ($n$ = 4) is oriented toward CO with a binding energy of 2.0 kcal/mol. In all the clusters, the binding energies of CO to $(H_2O)_n$ were very small, indicating that the interaction of CO with $(H_2O)_n$ was weak. Similar structures were obtained at the CAM-B3LYP/6-311++G(d,p) level, as shown in Figure S1.


https://doi.org/10.1021/acsomega.1c02612
ACS Omega 2021, 6, 16688−16695

**3.2. Ionization of the CO−$H_2O$ 1:1 Complex.** First, the structure of the CO−$H_2O$ 1:1 complex was optimized at the MP2/6-311++G(d,p) level. The reaction dynamics of $[CO-H_2O]^+$, following the vertical ionization of the neutral CO−$H_2O$ complex, were calculated by the direct AIMD method at the MP2/6-311++G(d,p) level. The initial structure of $[CO-H_2O^+]_{ver}$ was chosen as the optimized structure of CO−$H_2O$ in this trajectory; $[M^+]_{ver}$ denotes the structure of $M^+$ at the vertical ionization point from neutral complex $M$.

Time evolution of the potential energy and snapshots of $[CO-H_2O]^+$ are shown in Figure 3. At time zero, the spin

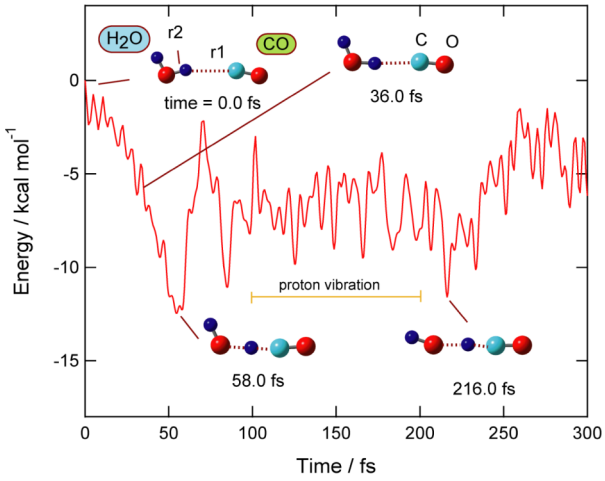


**Figure 3.** Time evolution of the potential energy and snapshots of $[CO(H_2O)]^+$ after vertical ionization of the neutral cluster of $CO(H_2O)$. Direct AIMD calculation was performed at the MP2/6-311++G(d,p) level. The MP2/6-311++G(d,p) optimized geometry was used as the initial geometry at time zero.

densities on $H_2O$ and CO were 1.00 and 0.00, respectively, indicating that the unpaired electron was fully localized on $H_2O$. At time zero, distances $r_1$ and $r_2$ were 2.445 and 0.961 Å, respectively. After ionization, the potential energy decreased gradually as a function of time. The energy was −6.6 kcal/mol at 36.0 fs, when $r_1$ and $r_2$ were 2.057 and 1.012 Å, respectively, indicating that the CO molecule gradually approached $H_2O$. At 58.0 fs, the energy was minimized at −12.3 kcal/mol, and the distances $r_1$ and $r_2$ were 1.200 and 1.332 Å, respectively, implying that the proton of $H_2O$ was transferred to the CO molecule via the formation of a $[HO-H-CO]^+$ species. Between 100 and 200 fs, the proton vibrated between OH and CO (proton vibration). At 216.0 s, the structure of $[HO-H-CO]^+$ ($r_1$ = 1.188 and $r_2$ = 1.481 Å) was close to that of its optimized structure ($r_1$ = 1.208 and $r_2$ = 1.436 Å), as shown in Figure S2. Thus, the ionization of the CO−$H_2O$ 1:1 complex resulted in the formation of a proton-transfer (PT) complex $[HO-H-CO]^+$, and the HOCO radical was not formed.

**3.3. Ionization of the $CO(H_2O)_n$ ($n$ = 2) Cluster.** Time evolution of the potential energy and snapshots of $CO(H_2O)_2^+$ are shown in Figure 4. The direct AIMD calculations were carried out at the MP2/6-311++G(d,p) level without ZPE. The water dimer was oriented toward CO at time zero. At the vertical ionization state, $[CO(H_2O)_2^+]_{ver}$, the charges on CO, $H_2O$(I), and $H_2O$(II) were calculated to be +0.002, +0.961, and +0.037, respectively. The spin densities on CO, $H_2O$(I), and $H_2O$(II) were 0.002, 1.000, and −0.002, respectively. These results indicated that the ionization occurred locally in $H_2O$(I). After

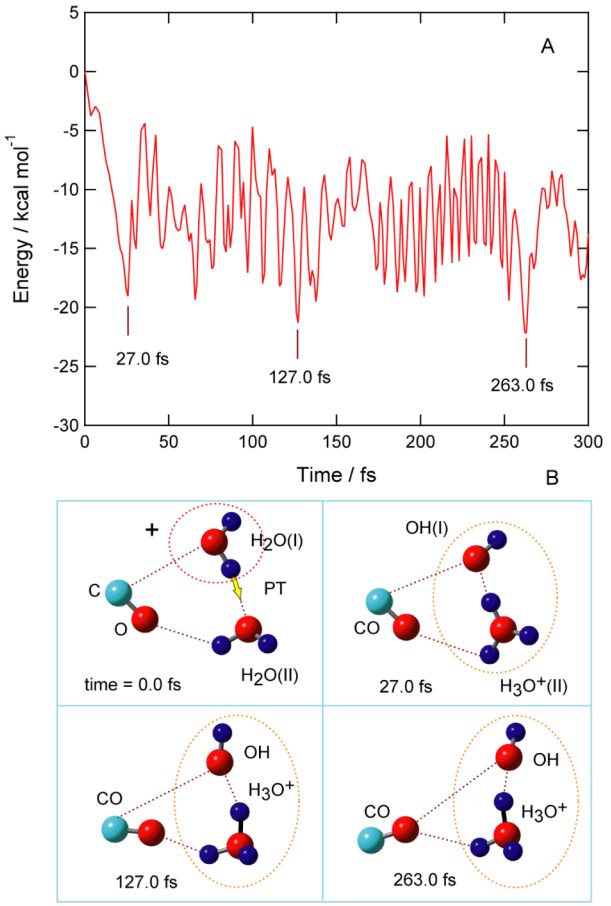


**Figure 4.** (A) Time evolution of the potential energy and (B) snapshots of $[CO(H_2O)_n]^+$ ($n$ = 2) after vertical ionization of the neutral cluster of $CO(H_2O)_n$. Direct AIMD calculation was performed at the MP2/6-311++G(d,p) level. The MP2/6-311++G(d,p) optimized geometry was used as the initial geometry at time zero.

ionization, the proton of $H_2O(I)^+$ was rapidly transferred to the oxygen atom of $H_2O$(II), and the ion−radical complex OH(I)−$H_3O^+$(II) was formed. The PT was complete at 27.0 fs, and the potential energy was −19.0 kcal/mol. The PT was followed by structural relaxation from 127 to 150 fs. In the final stage of the reaction (263.0 fs), a complex consisting of $CO(H_3O^+)OH$ was formed.

Thus, the HOCO radical was not formed from the ionization of $CO(H_2O)_2$. Only PT was observed as well as that in water dimer cation without CO. CO is a mere spectator in the ionization of $CO(H_2O)_n$. The ionization occurs in water molecules because the ionization potential of $H_2O$ ($I_p$ = 12.65 eV) is lower than that of CO ($I_p$ = 14.01 eV). In addition, the proton of $H_2O^+$ was not transferred to CO but to $H_2O$ because the proton affinities of $H_2O$, CO, and OH are 170.8 (165.2), 149.3 (142.0), and 147.9 (141.8) kcal/mol, respectively, at the MP2/6-311++G(d,p) level; the values in parentheses correspond to the experimental ionization potential. It is evident that the proton affinity of $H_2O$ is significantly higher than that of CO, because of which the proton of $H_3O^+$ is preferentially transferred to $H_2O$.

Similar direct AIMD calculations were carried out for $CO(H_2O)_n$ ($n$ = 3 and 4). Snapshots and potential energies of $CO(H_2O)_n^+$ for $n$ = 3 and 4, following the ionization of neutral clusters, are shown in Figures S3 and S4, respectively. In both the clusters ($n$ = 3 and 4), only PT was observed within the water


https://doi.org/10.1021/acsomega.1c02612
ACS Omega 2021, 6, 16688−16695

cluster cation; the HOCO radical was not formed upon the ionization of the CO−$H_2O$ clusters.

The direct AIMD calculations for $CO(H_2O)_n$ ($n$ = 2−4) were also performed at the CAM-B3LYP/6-311++G(d,p) level for the optimized geometry. PT was observed for all clusters without ZPE.

**3.4. Effects of Thermal Activation of Structures of $CO(H_2O)_n$ ($n$ = 2−4) on the Reaction Mechanism.** In the previous sections, the MP2-optimized structures of $CO(H_2O)_n$ ($n$ = 2−4) were used in the initial geometries in the direct AIMD calculations. The effects of the initial geometry on the reaction dynamics are discussed in this section.

The initial geometries of $CO(H_2O)_n$ ($n$ = 2−4) were generated by the thermal activation at 10 K using direct AIMD calculations of the neutral clusters at the CAM-B3LYP/6-311++G(d,p) level. Ten trajectories were selected for each $n$ from the geometries at 10 K, and then direct AIMD calculations of $[CO(H_2O)_n^+]_{ver}$ were performed at the CAM-B3LYP/6-311++G(d,p) level. The results are given in Table 1. All the simulations indicated the formation of the PT product from the $CO(H_2O)_n$ cluster. The reaction can be expressed as

$$CO(H_2O)_n + IP \rightarrow [CO(H_2O)_n^+]_{ver} \rightarrow CO(H_3O^+)OH(H_2O)_{n-2}, \quad (n = 2-4)$$

**Table 1. Results of Direct AIMD Calculations of the $CO(H_2O)_n^+$ Systems[a]**

| $n$ | [MP2:MP2] | [CAM:CAM (10K)] | ZPE [CAM:CAM] |
|---|---|---|---|
| 2 | PT | PT[b] | PT[c] |
| 3 | PT | PT[b] | HOCO[b] |
| 4 | PT | PT[b] | HOCO[b] |

[a]PT denotes proton transfer. [MP2:MP2] denotes that the geometry of neutral cluster was obtained by the MP2/6-311++G(d,p) method (right) and the dynamics of $CO(H_2O)_n^+$ were calculated at the MP2/6-311++G(d,p) level (left). [CAM:CAM (10K)] denotes that the geometry of neutral cluster was obtained by the simulation of the neutral cluster at 10 K (CAM-B3LYP/6-311++G(d,p) level) (right) and the reaction dynamics of $CO(H_2O)_n^+$ were calculated at the MP2/6-311++G(d,p) level (left). ZPE denotes that direct AIMD calculations were carried out on $CO(H_2O)_n$ with ZPE. [b]Ten trajectories were run. [c]Thirty trajectories were run.

**3.5. Effects of ZPE of $CO(H_2O)_n$ ($n$ = 2−4) on Reaction Mechanism.** As reported in the previous sections, the MP2 and CAM-B3LYP optimized structures and the initial geometries of thermally activated structures of $CO(H_2O)_n$ ($n$ = 2−4) were examined via the direct AIMD calculations. The effects of ZPE on the reaction dynamics are discussed in this section.

First, the structure of $CO(H_2O)_n$ was optimized at the CAM-B3LYP/6-311++G(d,p) level. Next, ZPE energy was added to $CO(H_2O)_n$, and direct AIMD calculations were performed from the vertical ionization point.

The time evolution of the potential energy and snapshots of $[CO(H_2O)_3]^+$ are shown in Figure 5. At time zero, a hole was mainly localized on the $H_2O$(I) bonded to CO. Moreover, the distance between the carbon atom of CO and the oxygen atom of $H_2O(I)^+$ was $R$(C−O) = 3.523 Å at this time. After ionization, the potential energy gradually decreased as a function of time. The energy was −30.0 kcal/mol at 32.2 fs. This energy reduction was caused by the PT from $H_2O(I)^+$ to $H_2O$(II). The C−O distance was constant, that is, $R$(C−O) = 3.457 Å at 32.2 fs. After PT, the OH radical gradually approached CO between 50 and 200 fs. The C−O distance decreased to $R$(C−O) = 1.940 Å at 202.6 fs. The addition of OH radicals to CO occurred at 225.5 fs, and HOCO was formed. The energy decreased to −48.0 kcal/mol. Ten trajectories were run, and two reactive trajectories were obtained.

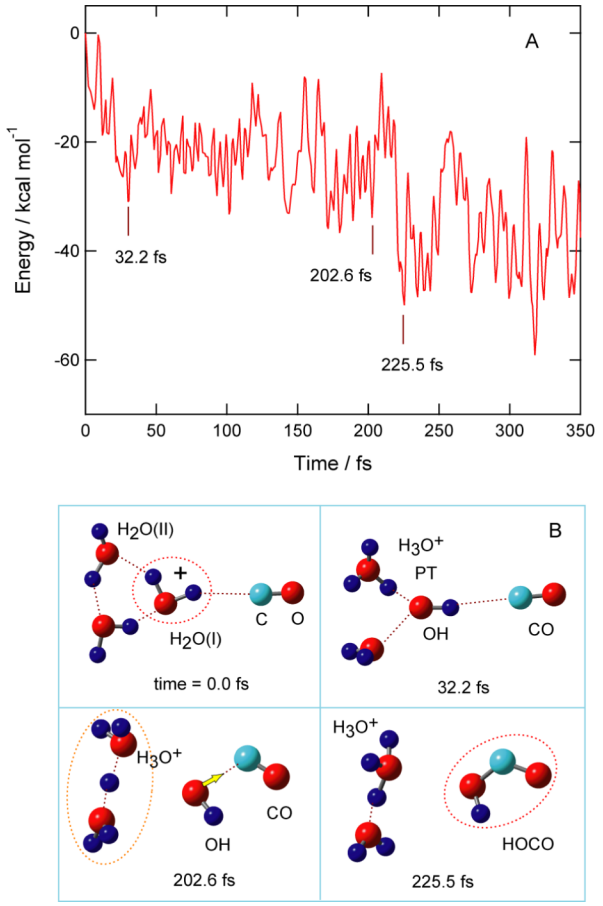


**Figure 5.** Effects of ZPE on the time evolution of (A) potential energy and (B) snapshots of $[CO(H_2O)_3]^+$ after vertical ionization of the neutral cluster of $CO(H_2O)_3$. Direct AIMD calculation was performed at the CAM-B3LYP/6-311++G(d,p) level.

Similar calculations were performed for $n$ = 2 and 4. The results are presented in Table 1. HOCO formation was observed when $n$ = 3 and 4. The time evolution of the potential energy and snapshots of $[CO(H_2O)_4]^+$ are shown in Figure S5. In contrast, HOCO was not formed when $n$ = 2, although 30 trajectories were run.

**3.6. Effects of Vibrational Excitation on the Reaction Dynamics of $CO(H_2O)_2$ Clusters.** In the previous sections, it was demonstrated that the HOCO radical was not formed from the reaction of $[CO(H_2O)_n^+]_{ver}$, following the ionization of parent neutral cluster $CO(H_2O)_n$ ($n$ = 1−4). In this section, the effect of vibrational excitation of the neutral cluster on the formation of the HOCO radical is discussed.

Figure 6 shows a sample trajectory for the formation of the HOCO radical from vibrationally excited $CO(H_2O)_2$. The initial structure of the vibrational excited states of $CO(H_2O)_2$ was chosen from the normal mode analysis. Figure S6A shows a normal mode vector of the intermolecular vibrational stretching between CO and water dimer $(H_2O)_2$ (55.5 $cm^{-1}$ at the MP2/6-311++G(d,p) level). This structure corresponds to one of the structures at the classical turning point on the potential energy curve (PEC) (the vibrational energy and quantum number were


https://doi.org/10.1021/acsomega.1c02612
ACS Omega 2021, 6, 16688−16695

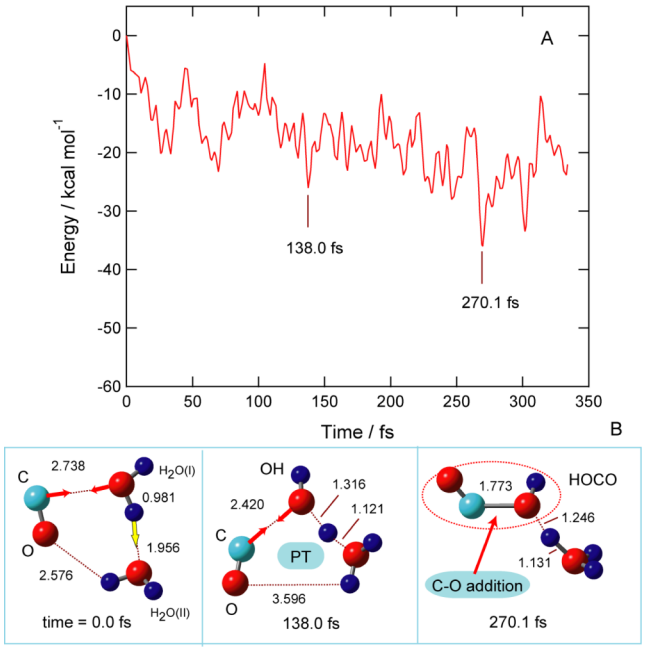


**Figure 6.** (A) Time evolution of the potential energy and (B) snapshots of $[CO(H_2O)_2]^+$ after vertical ionization of the neutral cluster of the vibrationally excited $CO(H_2O)_2$ (see text). The initial geometry for the direct AIMD calculation was performed at the MP2/6-311++G(d,p) level.

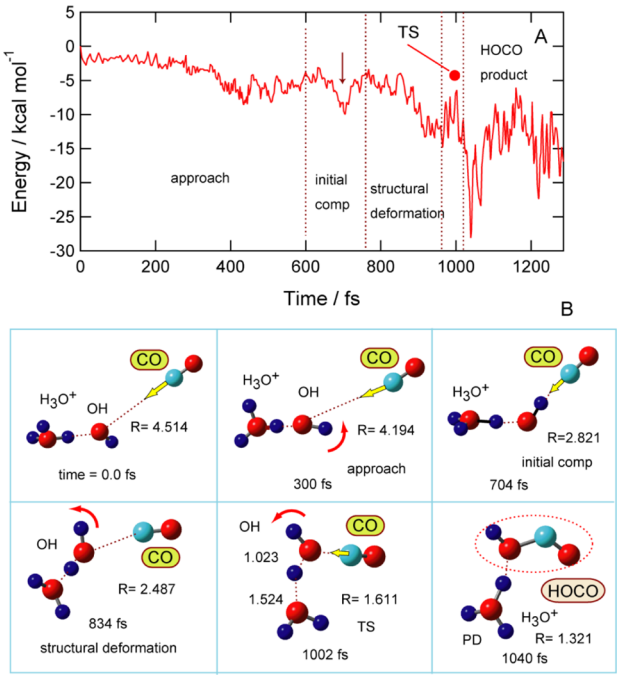


**Figure 7.** (A) Time evolution of the potential energy for the collision reaction of CO + $(H_2O)_n$ ($n$ = 2) and (B) snapshots of the reaction of CO + $(H_2O)_n^+$ ($n$ = 2). Direct AIMD calculation was performed at the CAM-B3LYP/6-311++G(d,p) level. The CAM-B3LYP/6-311++G-(d,p) optimized geometry was used as the initial geometry at time zero. The collision energy was zero.

3.0 kcal/mol and $v$ = 20, respectively), as shown in Figure S6B. Intermolecular distance $R$ was 2.738 Å, which was significantly shorter than that for the optimized structure of $CO(H_2O)_2$ ($R$ = 3.330 Å). After ionization of the vibrational excited states of $CO(H_2O)_2$, the spin density was distributed on both CO and $H_2O$(I): the spin densities on CO, $H_2O$(I), and $H_2O$(II) were calculated to be 1.159, −0.161, and 0.002, respectively. This is remarkably different from that observed for the vibrational ground state—there is no spin density on CO. After the ionization, a proton from $H_2O$(I) was gradually transferred to $H_2O$(II) at 138.0 fs, and CO approached $H_2O$(I) at the same time. The distances of CO from $H_2O$(I) were 2.738 Å (time = 0) and 2.420 Å (138.0 fs). CO further approached OH in the time range of 150−250 fs. At 270.1 fs, the HOCO radical was formed, and the energy was −35.0 kcal/mol. Thus, vibrational excitation of the intermolecular stretching mode led to the formation of the HOCO radical.

Several other vibrational modes were examined. However, all the trajectories indicated only PT in the water cluster cation.

### 3.7. Collision Reaction between CO and $(H_2O)_n^+$ ($n$ = 2).

In this section, the bimolecular collision reaction between CO and $(H_2O)_n^+$ ($n$ = 2) was examined. Calculations were carried out at the CAM-B3LYP/6-311++G(d,p) level, because collision reactions require longer simulation time. The collision energy was zero ($E_{coll}$ = 0.0 kcal/mol). Time evolution of the potential energy and snapshots for the sample reactive trajectory of CO + $(H_2O)_2^+$ are given in Figure 7. The chemical structure of the water dimer cation is expressed as $H_3O^+$(OH). At time zero, CO was located at a distance $R$ = 4.514 Å from the water dimer cation $H_3O^+$(OH), where $R$ is the distance between the carbon atom of CO and the oxygen atom of OH. After initiation of the reaction, CO approached gradually to the OH radical of the water dimer cation; distances $R$ were 4.360 Å at 200 fs and 4.194 Å at 300 fs. The OH radical was gradually oriented toward CO. At 704.0 fs, CO was bound to the hydrogen atom of OH with $R$ = 2.821 Å. The weak OH−CO bond was generated during the formation of the initial complex, and the energy decreased to −9.0 kcal/mol.

Next, structural deformation occurred within the cluster (834 fs). The energy was gradually stabilized (−15.0 kcal/mol). The structure at 1002 fs was close to that of the transition state (TS) formed during the addition of CO to OH (Figure S7). The carbon atom of CO attacked the oxygen atom of OH at 1002 fs. The potential energy suddenly decreased beyond TS due to the formation of the strong C−O bond between CO and the OH radical. The HOCO radical was formed as the HOCO−$H_3O^+$ complex at the final stage (1040 fs).

### 3.8. Collision Reaction between CO and $(H_2O)_n^+$ ($n$ = 3).

A sample trajectory for reactive bimolecular collision, CO + $(H_2O)_n^+$ ($n$ = 3), is given in Figure 8. In this trajectory, CO was located at the region of the OH radical of the water cluster cation. The collision energy was zero ($E_{coll}$ = 0.0 kcal/mol). At time zero, CO was located at a distance $R$ = 4.234 Å from OH. The zero level of energy corresponds to the total energy of reactants CO and $(H_2O)_3^+$. After the initiation of the reaction at time zero, CO approached gradually to OH; the distances $R$ were 4.113 Å (300 fs) and 3.454 Å (600 fs), and the potential energy was almost constant during this time (0−600 fs). At 673 fs, an initial complex in which CO contacts OH of the water trimer cation was formed, and the energy decreased to −4.5 kcal/mol. The carbon atom of CO interacts with a hydrogen atom of OH in the initial complex with $R$ = 3.128 Å. Next, structural deformation occurred at 800 fs. At 901 fs, the structure of the CO−OH−$H_2O$ moiety was close to that of TS formed during the addition of CO to OH. The reaction point reached to TS. Beyond TS, the energy decreased suddenly to −22.0 kcal/mol, where the HOCO radical was formed by the collision of


https://doi.org/10.1021/acsomega.1c02612
ACS Omega 2021, 6, 16688−16695

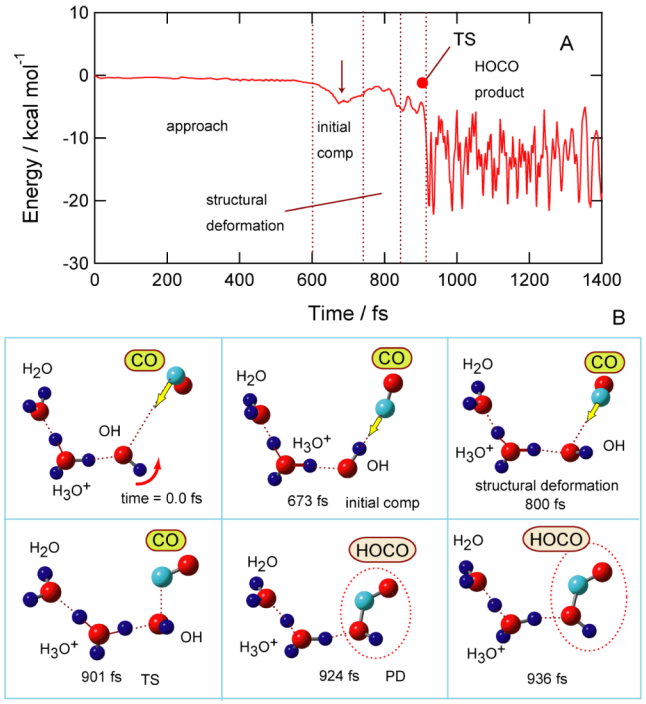


**Figure 8.** (A) Time evolution of the potential energy for the collision reaction of CO and $(H_2O)_n$ ($n$ = 3) and (B) snapshots of the reaction between CO and $(H_2O)_n^+$ ($n$ = 3). Direct AIMD calculation was performed at the CAM-B3LYP/6-311++G(d,p) level. The CAM-B3LYP/6-311++G(d,p) optimized geometry was used as the initial geometry at time zero. The collision energy was zero.

CO on OH at 924 fs. The formation of HOCO was complete at 936 fs, and the HOCO−$H^+(H_2O)_2$ complex was formed.

The sample trajectory for $n$ = 4 is shown in Figure S8. PT was found as well as $n$ = 2 and 3. Summary of all trajectory calculations for CO + $(H_2O)_n^+$ ($n$ = 2−3) is given in Table S1. "Reactive" means a reactive trajectory leading to HOCO, and "nonreactive" means the reaction remained in CO−$(H_2O)_n^+$ intermediate complex (IM).

**3.9. Energy Diagram.** Potential energy diagram for the formation of the HOCO radical is given in Figure 9. The relative energies in the $CO(H_2O)_n$ ($n$ = 2) system were calculated at the MP2 and CCSD(T) levels of theory with the 6-311++G(d,p) basis set. The energy diagram consisted of two reaction channels: collision reaction denoted as "collision reaction" and HOCO formation from the ionization of the neutral cluster of $CO(H_2O)_n$, denoted as "reaction after ionization." The zero level of energy is assumed to be the total energy of IM, denoted as $CO(H_2O)_n^+$. In the collision reaction, the initial energy level of reactants CO and $(H_2O)_n^+$ ($n$ = 2) was 12.2 kcal/mol higher than that of IM. The HOCO radical is formed via IM and TS with a reaction energy of −12.2 kcal/mol relative to the energy level of IM.

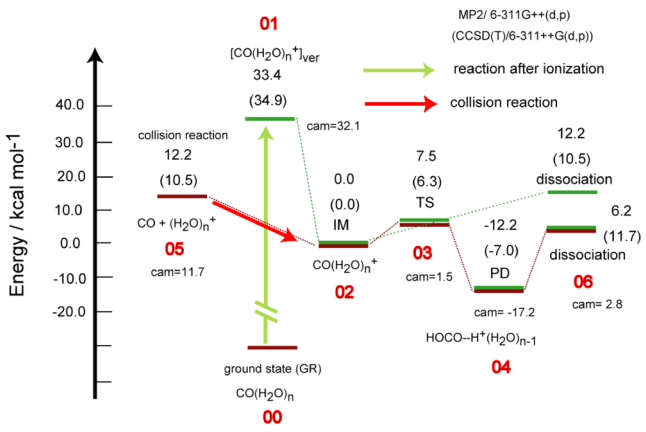


**Figure 9.** Energy diagram of the $CO(H_2O)_n^+$ system. The calculations were performed at the MP2 and CCSD(T) levels with the 6-311++G(d,p) basis set. The values denote relative energies (in kcal/mol) calculated at the MP2/6-311++G(d,p) level. The relative energies (in kcal/mol) at the CCSD(T)/6-311++G(d,p) level are given in parentheses.

In case of the reaction after ionization, the vertical ionization point has a large excess of energy relative to IM (33.4 kcal/mol) and TS (25.9 kcal/mol). However, the direct AIMD calculations showed that the reaction point did not exceed over TS and was still limited to the IM region. This was because only PT occurred within the water cluster, and CO behaved as a spectator in the reaction system. The HOCO radical could not be formed from the ionization of neutral cluster $CO(H_2O)_n$ ($n$ = 2−4) within 2 ps time scale.

The relative energies were also calculated at the CCSD(T)/6-311++G(d,p) level and are given in parentheses. The energetics of CCSD(T) were in good agreement with those of MP2. The relative energies for $n$ = 3 and 4 were calculated and are given in Table S2. The activation energies for $n$ = 3 and 4 were 9.0 and 6.7 kcal/mol, respectively, indicating that the size dependency of the barrier height was small in the present system.

Based on the static ab initio calculations and the Rice−Ramsperger−Kassel−Marcus (RRKM) theory, the reaction rates were calculated in the case of zero excess energy of $[CO(H_2O)_n]_{ver}$ ($E_{ex}$ = 0.0 eV) and an excess energy of 11.98 eV ($E_{ex}$ = 11.98 eV), which are generated by a hole transfer reaction, that is, $He^+ + H_2O \rightarrow H_2O^+ + He + 11.98$ eV. The results are presented in Table S3. The RRKM reaction rates when $E_{ex}$ = 0.0 and 11.98 eV were $6.65 \times 10^{10}$ and $1.43 \times 10^{12}$ $s^{-1}$, respectively. The excess energy resulting from the hole transfer accelerates the formation of HOCO.

## 4. DISCUSSION AND CONCLUSIONS

**4.1. Comparison with Experiments.** Liu et al. investigated the bimolecular reactions induced by electron impact ionization in helium droplets.[15−17] They observed the reactions $X$ + $(H_2O)_n^+$ ($X$ = CO, Ar, $CO_2$, $O_2$, and $N_2$). For $X$ = Ar, $CO_2$, $N_2$, and $O_2$, the parent water cluster cation $(H_2O)_n^+$ was detected after the ionization of $X(H_2O)_n$. In contrast, for $X$ = CO, the protonated water cation $H^+(H_2O)_{n-1}$ was detected after the ionization of $X(H_2O)_n$, indicating that CO behaved in a different manner in helium droplets. The present calculations show that the ion−molecule reaction CO + $(H_2O)_n^+ \rightarrow H^+(H_2O)_{n-1}$ + HOCO proceeds effectively, with a very short reaction time (<2 ps). In addition, the ionization of $CO(H_2O)_n$ clusters leads to the formation of HOCO. The present calculations strongly support the experimental observations in helium droplets.[15−17]

**4.2. Conclusions.** The PECs for the formation of the HOCO radical are schematically illustrated in Figure 10. The upper curves correspond to the PEC for the bimolecular collision reaction between CO and $(H_2O)_n^+$. The approach of CO to $(H_2O)_n^+$ decreases the potential energy of the reaction system gradually with the decrease in intermolecular distance between CO and $(H_2O)_n^+$. IM, CO−$(H_2O)_n^+$, is first formed by the collision of CO to $(H_2O)_n^+$. CO is oriented toward the OH radical of $(H_2O)_n^+$. Following this, CO binds to OH, and the


https://doi.org/10.1021/acsomega.1c02612
ACS Omega 2021, 6, 16688−16695

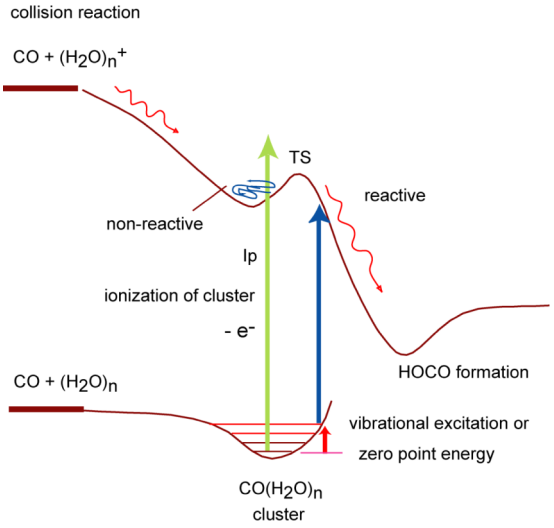


**Figure 10.** Schematic illustration of the potential energy curves for the formation of HOCO after the vertical ionization of $CO(H_2O)_n$ ($n$ = 2–4) and after the collision reaction of CO and $(H_2O)_n^+$.

HOCO radical is formed via TS, $CO{-}OH{-}H^+(H_2O)_{n-1}$. The PEC for the collision reaction is a down-hill curve.

The reaction from the cluster comprising $CO(H_2O)_n$ corresponds to half-reaction of the bimolecular collision reaction. The reaction of $[CO(H_2O)_n^+]_{ver}$, following the ionization of the parent neutral cluster $CO(H_2O)_n$, starts from the equilibrium point of $CO(H_2O)_n$, as indicated by the green arrow. The vertical ionization point, $[CO(H_2O)_n^+]_{ver}$, is energetically higher than the TS. However, the structure of $[CO(H_2O)_n]_{ver}^+$ is considerably different from that of the TS: CO does not orient toward the OH radical formed by ionization. Therefore, HOCO is not formed, and the $CO(H_3O^+)(OH)(H_2O)_{n-2}$ complex is still limited to the IM region. If ZPE is added to the clusters or the vibrational mode corresponding to intermolecular stretching vibration between CO and $(H_2O)_2$ is excited in the neutral cluster of $CO(H_2O)_2$ (red arrow), the vertical ionization point shifts to the product region from TS. Therefore, the HOCO radical is formed from the $CO(H_2O)_2$ cluster by ionization (blue arrow).

This study suggests that the HOCO radical is formed from (1) the collision reaction of CO and $(H_2O)_n^+$, (2) the ionization of the $CO(H_2O)_n$ cluster ($n$ = 3 and 4) with ZPE, and (3) the ionization of the vibrationally excited $CO(H_2O)_n$ cluster (only found for $n$ = 2). In helium droplets, $CO(H_2O)_n^+$ has a large excess energy resulting from a hole transfer reaction, $He^+ + H_2O \rightarrow H_2O^+ + He + 11.98$ eV. This excess energy is dissipated into the vibrational modes of $CO(H_2O)_n$ and $CO(H_2O)_n^+$. Hence, HOCO may be formed in helium droplets. This study demonstrated that vibrational energy plays a crucial role in the formation of HOCO in $CO(H_2O)_n$ clusters.

## ■ ASSOCIATED CONTENT

### Supporting Information

The Supporting Information is available free of charge at https://pubs.acs.org/doi/10.1021/acsomega.1c02612.

Optimized structures of the neutral clusters $CO(H_2O)_n$ ($n$ = 1–4) calculated at the CAM-B3LYP/6-311++G(d,p) level; optimized structures of the $CO{-}H_2O^+$ complex cation calculated at the MP2/6-311++G(d,p) level; time evolution of the potential energy and snapshots of $[CO(H_2O)_3]^+$ after vertical ionization of the neutral cluster of $CO(H_2O)_3$; time evolution of the potential energy and snapshots of $[CO(H_2O)_4]^+$ after vertical ionization of the neutral cluster of $CO(H_2O)_4$; optimized structures of $CO(H_2O)_n^+$ ($n$ = 2) at TS for OH addition to CO calculated at the MP2/6-311++G(d,p) level; time evolution of the potential energy for the collision reaction of CO + $(H_2O)_n$ ($n$ = 4) and snapshots of the reaction of CO + $(H_2O)_n^+$ ($n$ = 4); optimized structures of the neutral cluster $CO(H_2O)_n$ ($n$ = 2) and displacement vector of intermolecular stretching mode between CO and water dimer calculated at the MP2/6-311++G(d,p) level; summary of trajectory calculations in the collision reactions, CO + $(H_2O)_n^+$; and relative energies ($\Delta E$ in kcal/mol) in $CO(H_2O)_n$ systems ($n$ = 2–4) calculated at the MP2 and CCSD(T) with 6-311++G(d,p) basis set (PDF)

## ■ AUTHOR INFORMATION


### Corresponding Author

**Hiroto Tachikawa** − *Division of Applied Chemistry, Faculty of Engineering, Hokkaido University, Sapporo 060-8628, Japan;* orcid.org/0000-0002-7883-2865; Email: hiroto@eng.hokudai.ac.jp

Complete contact information is available at: https://pubs.acs.org/10.1021/acsomega.1c02612


### Notes

The author declares no competing financial interest.

## ■ ACKNOWLEDGMENTS

The author acknowledges the partial support from JSPS KAKENHI (Grant nos. 21K04973 and 18K05021).

## ■ REFERENCES


(1) Toennies, P.; Vilesov, A.; Whaley, B. Superfluid Helium Droplets: An Ultracold Nanolaboratory. *Phys. Today* **2001**, *54*, 31.

(2) Fárník, M.; Fedor, J.; Kocisek, J.; Lengyel, J.; Pluharova, E.; Poterya, V.; Pysanenko, A. Pickup and Reactions of Molecules on Clusters Relevant for Atmospheric and Interstellar Processes. *Phys. Chem. Chem. Phys.* **2021**, *23*, 3195−3211.

(3) Bisset, R. N.; Pena Ardila, L. A.; Santos, L. Quantum Droplets of Dipolar Mixtures. *Phys. Rev. Lett.* **2021**, *126*, No. 025301.

(4) Bottcher, F.; Schmidt, J.-N.; Hertkorn, J.; Ng, K. S. H.; Graham, S. D.; Guo, M.; Langen, T.; Pfau, T. New States of Matter with Fine-tuned Interactions: Quantum Droplets and Dipolar Supersolids. *Rep. Prog. Phys.* **2021**, *84*, No. 012403.

(5) Mauracher, A.; Echt, O.; Ellis, A. M.; Yang, S.; Bohme, D. K.; Postler, J.; Kaiser, A.; Denifl, S.; Scheier, P. Cold Physics and Chemistry: Collisions, Ionization and Reactions inside Helium Nanodroplets close to Zero K. *Phys. Rep.* **2018**, *751*, 1−90.

(6) Buchenau, H.; Knuth, E. L.; Northby, J.; Toennies, J. P.; Winkler, C. Mass Spectra and Time-of-Flight Distributions of Helium Cluster Beams. *J. Chem. Phys.* **1990**, *92*, 6875−6889.

(7) Callegari, C.; Lehmann, K. K.; Schmied, R.; Scoles, G. Helium Nanodroplet Isolation Rovibrational Spectroscopy: Methods and Recent Results. *J. Chem. Phys.* **2001**, *115*, 10090−10110.

(8) Stienkemeier, F.; Lehmann, K. K. Spectroscopy and Dynamics in Helium Nanodroplets. *J. Phys. B: At. Mol. Opt. Phys.* **2006**, *39*, R127.

(9) Choi, M. Y.; Douberly, G. E.; Falconer, T. M.; Lewis, W. K.; Lindsay, C. M.; Merritt, J. M.; Stiles, P. L.; Miller, R. E. Infrared Spectroscopy of Helium Nanodroplets: Novel Methods for Physics and Chemistry. *Int. Rev. Phys. Chem.* **2006**, *25*, 15−75.

(10) Kupper, J.; Merritt, J. M. Spectroscopy of Free Radicals and Radical Containing Entrance-channel Complexes in Superfluid Helium Nanodroplets. *Int. Rev. Phys. Chem.* **2007**, *26*, 249−287.
(11) Doppner, T.; Diederich, T.; Przystawik, A.; Truong, N. X.; Fennel, T.; Tiggesbaumker, J.; Meiwes-Broer, K. H. Chrging of Metal Clusters in Helium Droplets Exposed to Intense Femtosecond Laser Pulses. *Phys. Chem. Chem. Phys.* **2007**, *9*, 4639−4652.
(12) LaForge, A. C.; Drabbels, M.; Brauer, N. B.; Coreno, M.; Devetta, M.; Di Fraia, M.; Finetti, P.; Grazioli, C.; Katzy, R.; Lyamayev, V. Collective Autoionization in Multiply-Excited Systems: A Novel Ionization Process Observed in Helium Nanodroplets. *Sci. Rep.* **2014**, *4*, No. 3621.
(13) Ziemkiewicz, M. P.; Neumark, D. M.; Gessner, O. Ultrafast Electronic Dynamics in Helium Nanodroplets. *Int. Rev. Phys. Chem.* **2015**, *34*, 239−267.
(14) Fárník, M.; Toennies, J. P. Ion-Molecule Reactions in $^4$He Droplets: Flying Nano-Cryo-Reactors. *J. Chem. Phys.* **2005**, *122*, No. 014307.
(15) Liu, J.; Shepperson, B.; Ellis, A. M.; Yang, S. Core-Shell Effects in the Ionization of Doped Helium Nanodroplets. *Phys. Chem. Chem. Phys.* **2011**, *13*, 13920−13925.
(16) Shepperson, B.; Liu, J.; Ellis, A. M.; Yang, S. Ionization of Doped Helium Nanodroplets: Residual Helium Attached to Diatomic Cations and Their Clusters. *J. Phys. Chem. A* **2011**, *115*, 7010−7016.
(17) Shepperson, B.; Liu, J.; Ellis, A. M.; Yang, S. Communication: The Formation of Helium Cluster Cations Following the Ionization of Helium Nanodroplets: Influence of Droplet Size and Dopant. *J. Chem. Phys.* **2011**, *135*, No. 041101.
(18) Lee, H. M.; Youn, I.-S.; Kim, K. S. CO Capture and Conversion to HOCO Radical by Ionized Water Clusters. *J. Phys. Chem. A* **2014**, *118*, 7274−7279.
(19) Tachikawa, H.; Kawabata, H. Hydrogen Dissociation Dynamics from Water Clusters on Triplet-State Energy Surfaces. *J. Phys. Chem. A* **2020**, *124*, 8421−8428.
(20) Tachikawa, H.; Iyama, T. Proton Transfer Reaction Rates in Phenol-Ammonia Cluster Cation. *J. Phys. Chem. A* **2020**, *124*, 7893−7900.
(21) Tachikawa, H. Intermolecular Reactions in Ionized Ammonia Clusters: A Direct Ab Initio Molecular Dynamics Study. *J. Phys. Chem. A* **2020**, *124*, 1903−1910.
(22) Jiménez-Escobar, A.; Chen, Y.-J.; Ciaravella, A.; Huang, C.-H.; Micela, G.; Cecchi-Pestellini, C. X-ray Irradiation of $H_2O$ + CO Ice Mixtures with Synchrotron Light. *Astrophys. J.* **2016**, *820*, No. 25.
(23) Watanabe, N.; Kouchi, A. Measurements of Conversion Rates of CO to $CO_2$ in Ultraviolet-induced Reaction of Amorphous $D_2O$-($H_2O$)/CO Amorphouse Ice. *Astrophys. J.* **2002**, *567*, 651−655.
(24) Bennett, C. J.; Hama, T.; Kim, Y.-S.; Kawasaki, M.; Kaiser, R. I. Laboratory Studies on the Formation of Formic Acid (HCOOH) in Interstellar and Cometary Ices. *Astrophys. J.* **2011**, *727*, No. 27.
(25) De Barros, A. L. F.; Boduch, P.; Domaracka, A.; Rothard, H.; De Silveira, E. F. Radiolysis of Astrophysical Ices by Heavy Ion Irradiation: Destruction Cross Section Measurement. *Low Temp. Phys.* **2012**, *38*, 759−765.
(26) Yanai, T.; Tew, D.; Handy, N. A New Hybrid Exchange-correlation Functional Using the Coulomb-attenuating Method (CAM-B3LYP). *Chem. Phys. Lett.* **2004**, *393*, 51−57.
(27) Watts, J. D.; Gauss, J.; Bartlett, R. J. Coupled-Cluster Methods with Noniterative Triple Excitations for Restricted Open-Shell Hartree-Fock and Other General Single Determinant Reference Functions. Energies and Analytical Gradients. *J. Chem. Phys.* **1993**, *98*, 8718−8873.
(28) Frisch, M. J.; Trucks, G. W.; Schlegel, H. B.; Scuseria, G. E.; Robb, M. A.; Cheeseman, J. R.; Scalmani, G.; Barone, V.; Mennucci, B.; Petersson, G. A.; *Gaussian 09*, revision D.01; Gaussian, Inc.: Wallingford, CT, 2013.
(29) Tachikawa, H.; Iura, R.; Kawabata, H. Water-accelerated $\pi$-Stacking Reaction in Benzene Cluster Cation. *Sci. Rep.* **2019**, *9*, No. 2377.
(30) Tachikawa, H. Jahn-Teller Effect of the Benzene Radical Cation: A Direct Ab Initio Molecular Dynamics Study. *J. Phys. Chem. A.* **2018**, *122*, 4121−4129.
(31) Tachikawa, H. Activation of $CO_2$ in Photoirradiated $CO_2$-$H_2O$ Clusters: Direct Ab Initio Molecular Dynamics (MD) Study. *J. Phys. Chem. A* **2019**, *123*, 4743−4749.
(32) Tachikawa, H. Proton Transfer vs Complex Formation Channels in Ionized Formic Acid Dimer: A Direct Ab Initio Molecular Dynamics Study. *J. Phys. Chem. A* **2020**, *124*, 3048−3054.


https://doi.org/10.1021/acsomega.1c02612
*ACS Omega* 2021, 6, 16688−16695